Cell

Structure and Function of RbcX, an Assembly Chaperone for Hexadecameric Rubisco

Sandra Saschenbrecker,[1,2] Andreas Bracher,[1,2,*] Karnam Vasudeva Rao,[1] Bharathi Vasudeva Rao,[1] F. Ulrich Hartl,[1,*] and Manajit Hayer-Hartl[1,*]
[1] Department of Cellular Biochemistry, Max Planck Institute of Biochemistry, Am Klopferspitz 18, 82152 Martinsried, Germany
[2] These authors contributed equally to this work.
*Correspondence: mhartl@biochem.mpg.de (M.H-H.), uhartl@biochem.mpg.de (F.U.H.), bracher@biochem.mpg.de (A.B.)
DOI 10.1016/j.cell.2007.04.025

SUMMARY

After folding, many proteins must assemble into oligomeric complexes to become biologically active. Here we describe the role of RbcX as an assembly chaperone of ribulose-bisphosphate carboxylase/oxygenase (Rubisco), the enzyme responsible for the fixation of atmospheric carbon dioxide. In cyanobacteria and plants, Rubisco is an ~520 kDa complex composed of eight large subunits (RbcL) and eight small subunits (RbcS). We found that cyanobacterial RbcX functions downstream of chaperonin-mediated RbcL folding in promoting the formation of $RbcL_8$ core complexes. Structural analysis revealed that the 15 kDa RbcX forms a homodimer with two cooperating RbcL-binding regions. A central cleft specifically binds the exposed C-terminal peptide of RbcL subunits, enabling a peripheral surface of RbcX to mediate $RbcL_8$ assembly. Due to the dynamic nature of these interactions, RbcX is readily displaced from $RbcL_8$ complexes by RbcS, producing the active enzyme. The strategies employed by RbcX in achieving substrate specificity and efficient product release may be generally relevant in assisted assembly reactions.

INTRODUCTION

Molecular chaperones fulfill essential functions in protein biogenesis and quality control in all types of cell (Frydman, 2001; Hartl and Hayer-Hartl, 2002). Although the term "molecular chaperone" was coined to describe a role in assisting oligomeric protein assembly (Ellis, 2006), it is now commonly thought that chaperones are primarily involved with mediating polypeptide chain folding, essentially by preventing misfolding and aggregation of newly-synthesized and stress-denatured polypeptides. These mechanisms are well established, particularly for the Hsp70s and the chaperonins (Frydman, 2001; Hartl and Hayer-Hartl, 2002). By contrast, how cells ensure the efficient assembly of folded subunits into oligomeric complexes is not well understood, and surprisingly few examples of specific assembly chaperones are known (Ellis, 2006). Hexadecameric ribulose 1,5-bisphosphate carboxylase/oxygenase (Rubisco) in chloroplasts, the most abundant enzyme in nature, has been an important paradigm in studies of protein assembly. Indeed, this process was initially thought to be mediated by the chaperonin system because nonassembled large subunits of plant Rubisco were observed to cofractionate with the chloroplast chaperonin (Barraclough and Ellis, 1980; Roy, 1989). However, attempts to reconstitute Rubisco with chaperonin alone have failed (Tabita, 1999), suggesting that additional factors must participate in this process.

Rubisco catalyzes the initial steps of two opposing reaction pathways: photosynthetic carbon fixation (CO_2 as the substrate) and photorespiration (O_2 as the substrate; Andrews and Lorimer, 1987). The photosynthetic fixation of CO_2 results in the synthesis of usable sugars (Gutteridge and Gatenby, 1995) and thus is responsible for plant growth and yield. Three structural forms of assembly of otherwise closely homologous Rubisco subunits are known (Andersson and Taylor, 2003; Tabita, 1999): Form I found in plants and cyanobacteria is a hexadecamer, denoted as $RbcL_8S_8$, containing eight large subunits (RbcL: MW 50-55 kDa) and eight small subunits (RbcS: MW 12-18 kDa). The oligomer has a cylindrical shape with a diameter of ~110 Å and a height of 100 Å. Four small subunits cap the top and bottom of eight large subunits, which form a tetramer of dimers. The simpler form II Rubisco in some photosynthetic bacteria (e.g., *Rhodospirillum rubrum*) and dinoflagellates is a dimer of RbcL subunits. Form III, found in a thermophilic archaeon, consists of five RbcL dimers.

Chaperonins are large cylindrical complexes with ATPase activity. The GroEL-type chaperonins (Cpn60s) of bacteria, chloroplasts, and mitochondria consist of two heptameric rings of ~60 kDa subunits, each forming

a central cavity for the binding of nonnative protein substrate (Frydman, 2001; Hartl and Hayer-Hartl, 2002). They function together with factors of the GroES/Cpn10 family, single-ring assemblies of seven ~10 kDa subunits, which bind transiently to the ends of the chaperonin cylinder. ATP-dependent GroES association results in the encapsulation of a single molecule of unfolded protein inside the GroEL cavity for folding to occur unimpaired by aggregation. Whereas bacterial GroEL and the mitochondrial chaperonin are homo-oligomeric, the chloroplast chaperonin is composed of homologous α and β subunits. Moreover, plant chloroplasts have two types of cochaperone, Cpn10 and Cpn20, the latter consisting of a tandem repeat of Cpn10 units (Hill and Hemmingsen, 2001). These features may represent an adaptation to chloroplast-specific substrate proteins.

The folding and assembly of form II Rubisco from *R. rubrum* has been reconstituted with bacterial GroEL/GroES (Goloubinoff et al., 1989a). In this reaction Rubisco subunits fold inside the chaperonin cage, followed by dimerization upon release into solution (Brinker et al., 2001). Expression of cyanobacterial form I Rubisco of *Synechococcus* sp. PCC6301 (also known as *Anacystis nidulans*) in *E. coli* was reported to result in the chaperonin-dependent production of enzymatically active holoenzyme (Goloubinoff et al., 1989b). As shown in cyanobacteria, assembly of the $RbcL_8S_8$ complex is thought to involve the formation of $RbcL_8$ core particles, followed by the docking of unassembled small subunits (Andrews and Lorimer, 1985). Recently it has been reported that the product of the *rbcX* gene, present in the intergenic space between the *rbcL* and *rbcS* genes in several cyanobacteria (Larimer and Soper, 1993), enhances the production of enzymatically active Rubisco upon coexpression with *rbcL* and *rbcS* in *E. coli* (Emlyn-Jones et al., 2006; Li and Tabita, 1997; Onizuka et al., 2004). Partial inactivation of *rbcX* in *Synechococcus* sp. PCC7002 resulted in a substantial reduction in Rubisco solubility and activity (Onizuka et al., 2004). However, the *rbcX* gene was reported to be nonessential in *Synechococcus* sp. PCC7942 (Emlyn-Jones et al., 2006).

Here we report that cyanobacterial RbcX is a Rubisco assembly chaperone. Structural and mechanistic analysis of RbcX from *Synechococcus* sp. PCC7002 revealed that the 15 kDa protein functions as a homodimer by binding and stabilizing RbcL subunits subsequent to their interaction with chaperonin. RbcX recognizes specifically, via a central peptide-binding groove, a conserved C-terminal peptide of RbcL. This interaction and additional contacts mediated by a peripheral binding surface of RbcX assist in the efficient formation of $RbcL_8$ core complexes. The RbcL-RbcX interaction is dynamic, facilitating displacement of RbcX from $RbcL_8$ by RbcS subunits to produce the active holoenzyme. The interchangeability of RbcX proteins between species is limited, suggesting that RbcX coevolved with RbcL and RbcS. We find that RbcX homologs are also present in higher plants.

RESULTS

Sequential Action of Chaperonin and RbcX in Assembly of Syn7002 Rubisco

The chaperone requirement for the folding and assembly of cyanobacterial form I Rubisco from *Synechococcus* sp. PCC7002 (Syn7002) was assessed upon expression of Rubisco subunits in *E. coli* cells with normal and elevated chaperonin levels. Amounts of soluble protein were determined upon fractionation of cell extracts and immunoblotting. Formation of $RbcL_8S_8$ holoenzyme (Figure 1A) or $RbcL_8$ complexes (Figure 1B) was monitored by Native-PAGE and Rubisco activity assay. In wild-type cells, expression of Syn7002-RbcL from an IPTG-inducible plasmid did not result in soluble protein, irrespective of whether RbcS was coexpressed (Figures 1A and 1B, lane 1). Transient (~10-fold) overexpression of GroEL/GroES prior to induction of *rbcLS* or *rbcL* also failed to produce significant amounts of soluble RbcL (Figures 1A and 1B, lane 2). Assembled Rubisco and carboxylation activity were essentially absent (Figures 1A and 1B, lanes 1–2). In contrast, expression of the homologous Rubisco from *Synechococcus* sp. PCC6301 (Syn6301) resulted in the formation of substantial amounts of $RbcL_8S_8$ or $RbcL_8$ complexes which migrated as high molecular weight bands on Native-PAGE (Figure S1A; Goloubinoff et al., 1989b).

In Syn7002, the RbcL and RbcS subunit genes are located in an operon that also encodes the protein RbcX in the order *rbcL-rbcX-rbcS*. Indeed, the assembly of Syn7002-$RbcL_8S_8$ proved to be critically dependent on coexpression of RbcLS with RbcX (Figure 1A, lane 3; Onizuka et al., 2004). Importantly, when Syn7002-RbcL was expressed in the absence of RbcS, RbcX was required for the formation of $RbcL_8$ core complexes competent for assembly to active enzyme with RbcS (Figure 1B, lane 3). Thus, RbcX appears to be required predominantly or exclusively for $RbcL_8$ formation. Overexpression of GroEL/GroES in the presence of RbcX caused a 3- to 4-fold increase in Syn7002 Rubisco activity, correlating with an increased amount of $RbcL_8S_8$ or $RbcL_8$ detected by Native-PAGE (Figures 1A and 1B, lane 4). In the case of Rubisco from Syn6301, where *rbcX* is encoded outside the *rbcLS* operon, assembly of $RbcL_8$ was enhanced 4- to 5-fold by RbcX coexpression (Figure S1B). Thus, RbcX strongly increases the yield of assembly but is not essential for $RbcL_8$ formation, at least in the case of Syn6301 Rubisco.

The requirement of GroEL/GroES and RbcX for efficient assembly was reproduced upon in vitro synthesis of Syn7002-RbcL in an *E. coli* translation lysate (Agashe et al., 2004; Figure 1C, lanes 1 and 2). Supplementing GroEL/GroES, but not GroES alone, together with RbcX produced mostly soluble RbcL and greatly increased the formation of $RbcL_8$ core complexes (Figure 1C, lanes 3 and 4). Rubisco activity was detected upon addition of purified RbcS (data not shown). RbcL translation in GroEL-immunodepleted lysate did not produce $RbcL_8$,

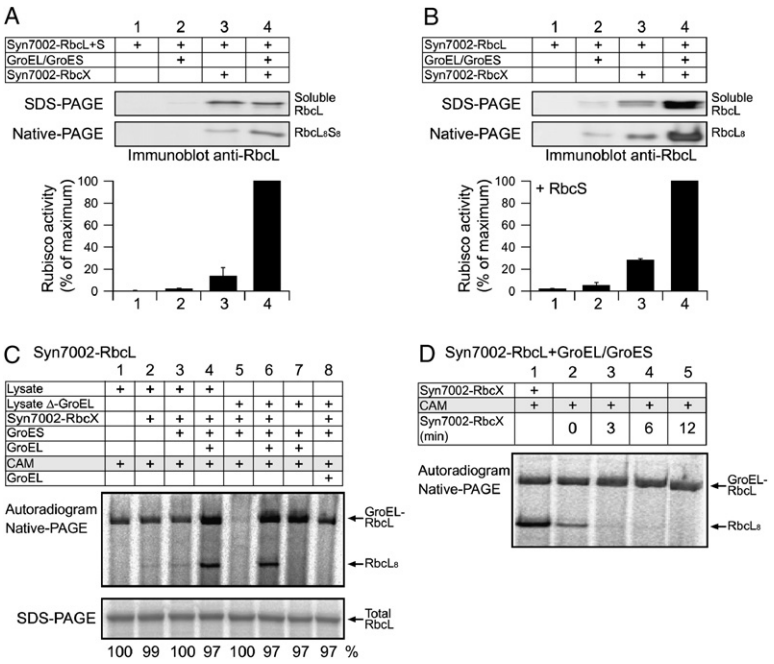

Figure 1. Requirement of the Chaperonin System and RbcX for Rubisco Assembly

(A and B) Syn7002-RbcL and RbcS (A) or Syn7002-RbcL (B) were expressed in *E. coli* with or without coexpression of Syn7002-RbcX and GroEL/GroES as indicated. RbcL in soluble cell lysates was analyzed by SDS-PAGE and $RbcL_8S_8$ or $RbcL_8$ complexes by Native-PAGE and immunoblotting. Carboxylation activity was measured directly in soluble cell lysates (A) or upon addition of purified RbcS (B). Activities measured upon coexpression with GroEL/GroES and RbcX are set to 100%. Error bars indicate standard deviation of three independent experiments.

(C) Syn7002-RbcL was translated in *E. coli* lysate in vitro in the presence of ^{35}S-Met (1.5 hr, 30°C). When indicated, GroEL/GroES (0.5 μM/1.0 μM) and Syn7002-RbcX (40 μM) were added to normal lysate (lanes 1–4) or GroEL-depleted lysate (Δ-GroEL, lanes 5–8). In lane 8, GroEL was added after stopping translation with CAM. Assembled $RbcL_8$ and total RbcL protein were analyzed by Native-PAGE and SDS-PAGE, respectively, followed by autoradiography.

(D) Syn7002-RbcL was translated in the presence of GroEL/GroES as in (C). RbcX was either present during translation (lane 1), was added together with CAM (lane 2) or after CAM addition (lanes 3–5), and assembled $RbcL_8$ was analyzed by Native-PAGE.

even when RbcX was present, demonstrating the requirement of both factors (Figure 1C, lanes 5–7). Importantly, readdition of GroEL after inhibition of RbcL translation with chloramphenicol (CAM) failed to produce $RbcL_8$ despite the presence of RbcX during translation (Figure 1C, lane 8). Note that some RbcL was bound to GroEL under these conditions, but this protein was not productive for folding. Thus, RbcX cannot stabilize RbcL for subsequent productive interaction with GroEL, suggesting that GroEL must interact with RbcL immediately upon synthesis. Indeed, while the production of $RbcL_8$ was most efficient when the lysate was supplemented with both GroEL/GroES and RbcX during translation (Figure 1D, lane 1), addition of RbcX immediately after blocking translation still mediated $RbcL_8$ formation, albeit at a reduced level (Figure 1D, lane 2). Delayed posttranslational addition of RbcX resulted in the rapid loss of RbcL assembly and in the formation of insoluble RbcL (Figure 1D and data not shown). Together these experiments indicate that RbcX has a specific chaperone function in preventing RbcL misassembly downstream of chaperonin.

Crystal Structure of RbcX

To understand the mechanism of RbcX action in Rubisco assembly, we undertook a structural analysis of Syn7002-RbcX by X-ray crystallography. RbcX was expressed in *E. coli* as a soluble protein of 15 kDa on SDS-PAGE. Analysis by multiangle light scattering indicated that RbcX forms a dimer of 30.2 kDa (Figure S2), henceforth referred to as RbcX. RbcX readily crystallized in space group $P4_12_12$ with three dimers in the asymmetric unit, and the structure was solved by Pt-SIRAS at a resolution of 2.8 Å (crystallographic data are summarized in Table S1). Residues 115 to 134 were not resolved in any of the RbcX peptide chains. Indeed, limited proteolysis of RbcX resulted in the removal of the poorly conserved 25 C-terminal residues (Figure S3), leaving a stable core domain of residues 1–109 (RbcX(ΔC25)) which was active in Rubisco assembly (Figure S4). We also solved the structure of SeMet-labeled RbcX(ΔC25) containing six RbcX dimers per asymmetric unit (Table S1). The average rms deviation for Cα positions between RbcX dimers in the crystal lattices was 0.623 Å, indicating that the core domain structure is rather rigid (Figure S5).

RbcX consists of four α helices per monomer (α1–4) that form an unusual helix bundle (Figure 2A). α2 (residues 35–48) turns backward relative to α1 (residues 4–33) with a steep interhelical angle of 151° and only one residue (N34) forming the turn. A very similar arrangement is observed at the junction between α3 (residues 52–63) and α4 (residues 65–107; interhelix angle 161°). The short helices α2 and α3 are connected by a five-residue linker. The core of the helical bundle is composed of conserved hydrophobic residues (Figure S3) without authentic coiled-coil side-chain packing. α4 makes an ~60° kink in the vicinity of residue 84 and forms a 35 Å long extension (α4C) pointing away from the helix bundle (Figure 2A). The RbcX dimer has overall dimensions of ~64 × 33 × 31 Å (length × height × width). The long α4 helices of the protomers align in an almost antiparallel fashion such that the

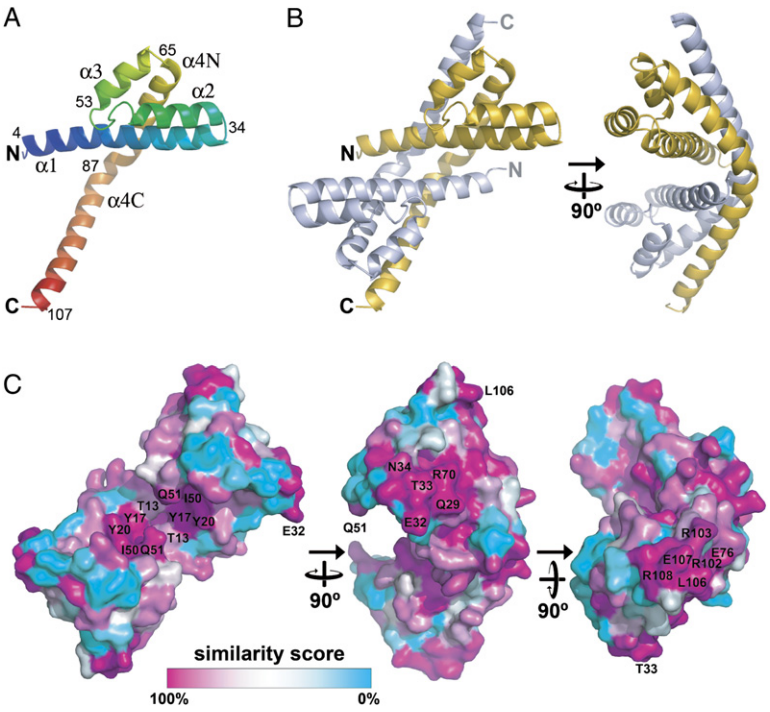

Figure 2. Crystal Structure of Syn7002-RbcX

(A) Ribbon representation of the RbcX monomer. The peptide backbone is depicted from N to C terminus using a color gradient from blue to red. Secondary structure elements, selected residue numbers, and chain termini are indicated.

(B) Structure of the RbcX dimer. Protomers are shown in yellow and blue.

(C) Surface conservation in RbcX. The similarity score from an alignment of 151 sequences of cyanobacterial RbcX in the PFAM database was plotted onto the accessible surface of the RbcX dimer. Sequence conservation is indicated by a color gradient, indicating highly conserved residues in magenta and variable regions in cyan. The positions of conserved surface residues are indicated.

helical bundles are located at opposite ends (Figure 2B). The α1 helices form additional symmetrical contacts and together with the α2 helices delineate a narrow diagonal groove in the arc-shaped complex. The dimer interface is predominantly uncharged and hydrophobic. A polar network around the conserved residue N98, contacting the amide backbone at position L72 and the side chains of R75 and E76 in the opposing protomer, contributes to dimer stability. The α2-α3 helical hairpins make no direct interchain contacts. Helix α2 is the most mobile element of the structure (Figure S5).

Crystallographic analysis of the RbcX from the cyanobacterium *Anabaena* sp. CA (AnaCA) revealed a structure virtually identical to that of Syn7002-RbcX (rmsd 1.14 Å over 103 Cα atoms; see Table S1 and Figure S6). Consistent with their high degree of sequence conservation (Figure S3), this suggests that all cyanobacterial RbcX homologs have the same overall architecture. The RbcX homologs identified in plants are more distant but share the register and the structural residues in the globular helix bundle of cyanobacterial RbcX (Figure S3).

Identification of Protein Interaction Surfaces on RbcX

Two highly conserved regions, representing potential protein-protein interaction sites, were identified on RbcX, the central groove of the dimer and a surface region around the corners of the molecule (Figure 2C). A hydrophobic area comprising the conserved residues Y17, Y20, and I50 of each monomer lines the groove in the center of the molecule (Figure 2C). Y17 packs against T13, which is frequently replaced in cyanobacterial RbcX sequences by an isosteric valine (Figure S3). Central access into the crevice is constricted to a 5.4 Å wide opening by the side chains of the highly conserved Q51 residues that is just wide enough to accommodate a polypeptide chain in an extended conformation. The other conserved region has predominantly polar character and is located at the corners of the RbcX dimer, comprising residues Q29, E32, T33, N34, R70, E76, and R102, R103, L106, E107, R108, respectively (Figure 2C). It is formed by helices 4 of both protomers and by the turn region between the α1 and α2 helices of one subunit and may serve to interact with a polar protein surface. Because of the 2-fold symmetry, this region occurs twice at opposing edges of the dimer.

The possible functional significance of these conserved regions of RbcX was investigated by mutational analysis (Figure 3A). Several single and double mutations predicted to compromise dimer formation failed to produce soluble RbcX and hence did not support the expression of soluble RbcL (Figure 3A, asterisks; Figure S7). All other RbcX mutant proteins were soluble and presumably had native-like dimer structure (Figure S7). A large set of mutations were of little or no effect on RbcL solubility and assembly (Figure 3A, circles). Individual alanine substitution of the central groove residues Y17 and Y20 reduced RbcL solubility and formation of $RbcL_8$ complexes (Figure 3A, lanes 6 and 7), while mutation of the adjacent residue T13 was without measurable effect (Figure 3A, lane 3). In contrast, the double mutation Y17A,Y20L abolished the formation of soluble RbcL almost completely (Figure 3A, lane 9). Since the crystal structure of this mutant protein

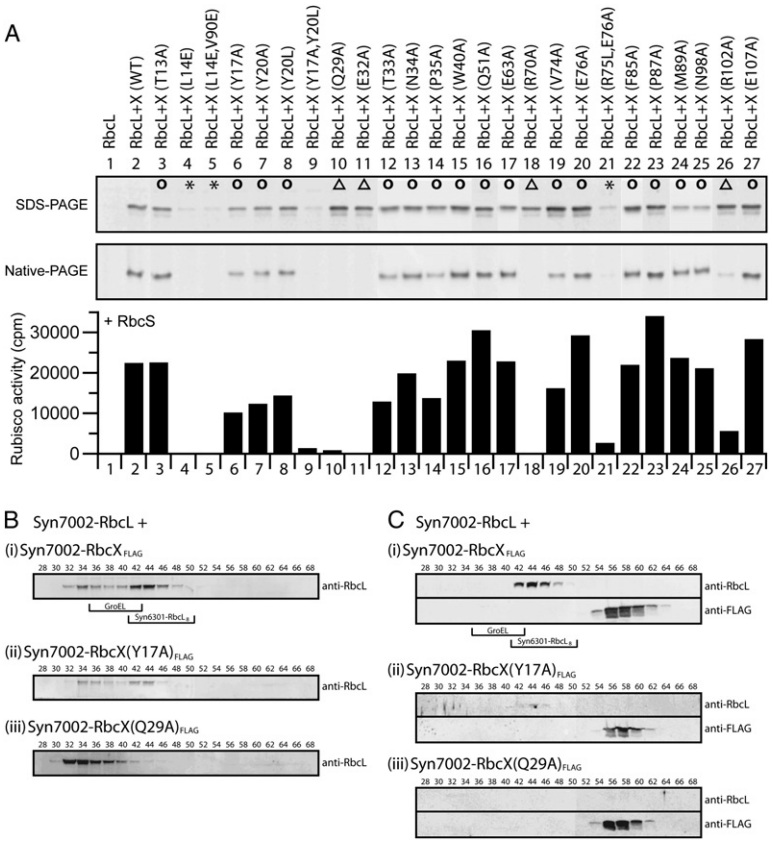

Figure 3. Functional Analysis of Syn7002-RbcX Mutants

(A) Soluble RbcL (SDS-PAGE), formation of $RbcL_8$ (Native-PAGE), and carboxylation activity were analyzed as in Figure 1B upon coexpression of Syn7002-RbcL in *E. coli* with wild-type and mutant RbcX proteins as indicated. (○), RbcX mutants supporting production of soluble and assembled RbcL; (*), RbcX mutants exhibiting poor solubility (see Figure S5); and (Δ), RbcX mutants supporting formation of soluble RbcL but little or no assembly of $RbcL_8$ and formation of active enzyme upon RbcS addition.

(B) Gel filtration analysis of soluble lysates prepared from *E. coli* cells coexpressing Syn7002-RbcL with (i) $RbcX_{FLAG}$, (ii) $RbcX(Y17A)_{FLAG}$, or (iii) $RbcX(Q29A)_{FLAG}$. Fractions were analyzed by SDS-PAGE and immunoblotted for RbcL. Elution of GroEL (~800 kDa) and Syn6301-$RbcL_8$ (~400 kDa) is indicated.

(C) Coimmunoprecipitation of RbcL with anti-FLAG antibody from cell lysates in (B), followed by native elution with FLAG peptide and gel filtration analysis as above. Fractions from gel filtration were immunoblotted for RbcL and $RbcX_{FLAG}$.

was virtually identical to that of wild-type RbcX (Table S1 and data not shown), this indicates that the central groove of RbcX has an essential function. Alanine substitution of the conserved residue Q51, which forms the upper rim of the central channel, was without detectable effect on RbcX function (Figure 3A, lane 16). Interestingly, several other individual mutations (Q29A, E32A, R70A, and R102A) allowed the accumulation of soluble RbcL but did not support assembly to $RbcL_8$ (Figure 3A, triangles). Notably, all of these mapped to the polar ends of the RbcX dimer, forming symmetrical, contiguous surfaces (Figure 2C).

The soluble RbcL produced upon coexpression with wild-type or mutant RbcX was analyzed by size-exclusion chromatography. Coexpression with N-terminally FLAG-tagged wild-type RbcX, which was fully active, resulted mainly in RbcL that fractionated at ~400 kDa, similar to a Syn6301-$RbcL_8$ standard (Figure 3Bi). A smaller amount of RbcL fractionated at a high molecular weight in excess of 800 kDa. This protein was not bound to GroEL and apparently represented misassembled, aggregated RbcL. No monomers of RbcL were detected, suggesting a high cooperativity of assembly. The RbcX mutant Y17A, partially impairing the function of the central groove, resulted in a reduced amount of $RbcL_8$ complex (Figure 3Bii). Interestingly, mutation Q29A, disrupting the peripheral polar surface of RbcX, supported exclusively the production of misassembled, high-molecular-weight RbcL (Figure 3Biii), confirming the absence of $RbcL_8$ complex upon analysis by Native-PAGE (Figure 3A, lane 10). Notably, RbcX did not detectably cofractionate with $RbcL_8$ (data not shown), suggesting either that the RbcL-RbcX interaction is labile on gel filtration or that RbcX binds to RbcL only transiently during $RbcL_8$ assembly. Coimmunoprecipitation from cell extracts with anti-FLAG antibody supported the former possibility. A substantial amount of RbcL was coimmunoprecipitated with $RbcX_{FLAG}$ but not with nontagged RbcX (data not shown). Following dissociation from the antibody by incubation with excess FLAG-peptide, the RbcL protein fractionated as the $RbcL_8$ complex (Figure 3Ci). Only a small amount of $RbcL_8$ coimmunoprecipitated with the mutant RbcX(Y17A), and no association was detectable with mutant RbcX(Q29A) (Figures 3Cii and 3Ciii), indicating that these mutations weakened the interaction of RbcX with RbcL, resulting in RbcL misassembly and aggregation.

In summary, these experiments identified two independent, functionally critical regions on RbcX, the central hydrophobic crevice and a peripheral polar surface of the molecule. Whereas the central crevice is essential for the production of soluble RbcL subunits, disruption of the polar surface results in the production of soluble but misassembled RbcL, suggesting a role in proper subunit arrangement.

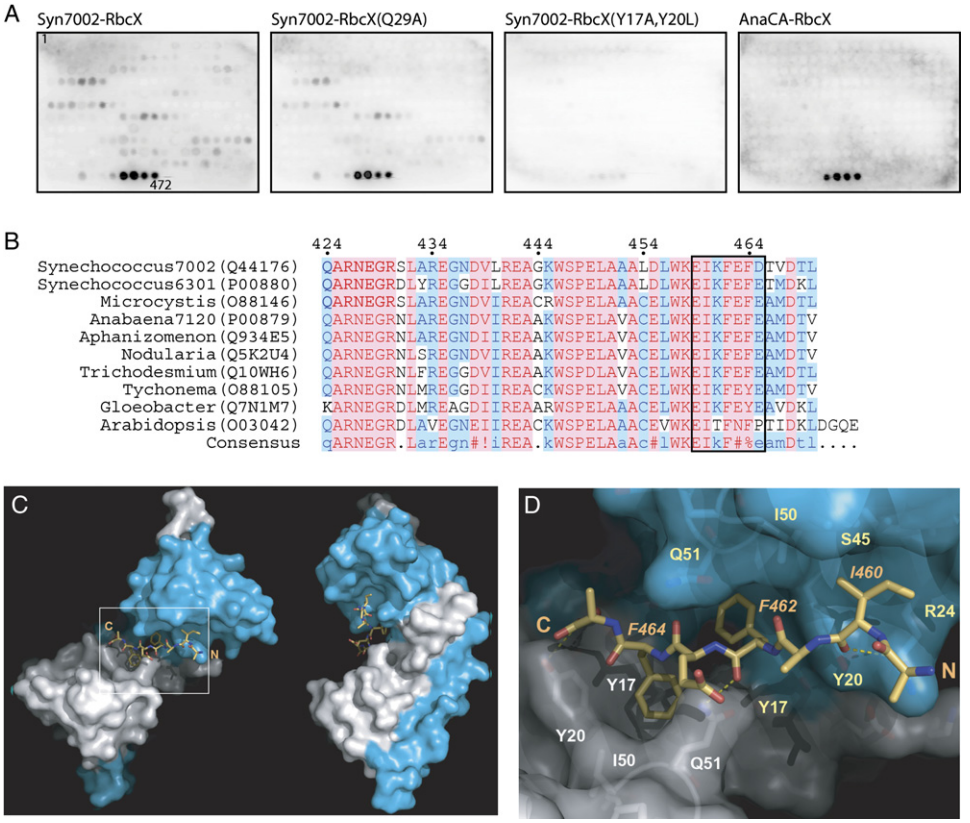

Figure 4. Binding of C-Terminal RbcL Peptide to RbcX

(A) A cellulose membrane containing an array of overlapping dodecamer peptides covering the sequence of Syn7002-RbcL was probed with the RbcX proteins indicated. Peptide-bound RbcX was visualized by chemiluminescent immunodetection with anti-RbcX antibody.

(B) Alignment using MultAlin (Corpet, 1988) of C-terminal amino acid sequences of RbcL from the cyanobacterial and higher plant species indicated (Swiss-Prot accession numbers in brackets). High consensus level ($\geq$ 90%) is depicted in red and low consensus level ($\geq$ 50%) in blue.

(C) Structure of the complex of peptide EIKFEFD bound to RbcX dimer. The peptide is shown in stick representation; RbcX is represented as a molecular surface with protomers colored white and blue, respectively. N and C termini of the peptide are indicated.

(D) Magnification of boxed area in (C) presenting a view of the refined peptide bound to RbcX. Molecular interactions between peptide and RbcX are highlighted. Dashed lines represent hydrogen bonds. Residues of the RbcX monomers participating in peptide binding are displayed in stick representation below the transparent surface of the molecule and are numbered in white and yellow, respectively. The important hydrophobic residues in the bound peptide are also labeled.

RbcX Binds the Conserved C-Terminal Peptide of RbcL

The structural features of the central groove region of RbcX seemed suitable for binding an extended peptide. To identify such a sequence element(s) in RbcL, an array of 12-amino-acid-long, acetylated peptides covering the entire sequence of Syn7002-RbcL with a ten residue overlap (231 peptides in total) was C-terminally attached to a cellulose-PEG membrane. Incubation with Syn7002-RbcX, followed by detection with anti-RbcX antibody, resulted in a strong binding signal with four RbcL peptides sharing the sequence EIKFEFD close to the C terminus of RbcL (Figures 4A and 4B). Other peptides exhibiting weaker binding had no apparent consensus motif. Essentially the same binding pattern was observed with the RbcX polar surface mutant Q29A, while the groove mutant Y17A,Y20L caused the complete loss of RbcX binding to the C-terminal RbcL peptide (Figure 4A). Specific binding to the C-terminal EIKFEFD motif was also detected with RbcX from *Anabaena* sp. CA (Figure 4A), suggesting that this interaction is a general property of cyanobacterial RbcX homologs. In the Rubisco holoenzyme, the C-terminal sequence of RbcL is located at the surface of the complex and has been implicated in regulating catalysis (Zhu et al., 1998). It is highly conserved among all form I Rubisco RbcL homologs (Figure 4B), including the proteins from higher plants, but is not found in archaeal and form II Rubisco (Figure S8A), along with the absence of RbcX in the respective organisms.

To obtain structural information on RbcL peptide binding, crystals of Syn7002-RbcX were soaked with the peptide EIKFEFD. One of the three crystallographically independent dimers in the native crystal form of RbcX exhibited difference electron density compatible with a bound peptide at the central recess (Figure S8B; Table S1). This difference density is not centered on the dyad

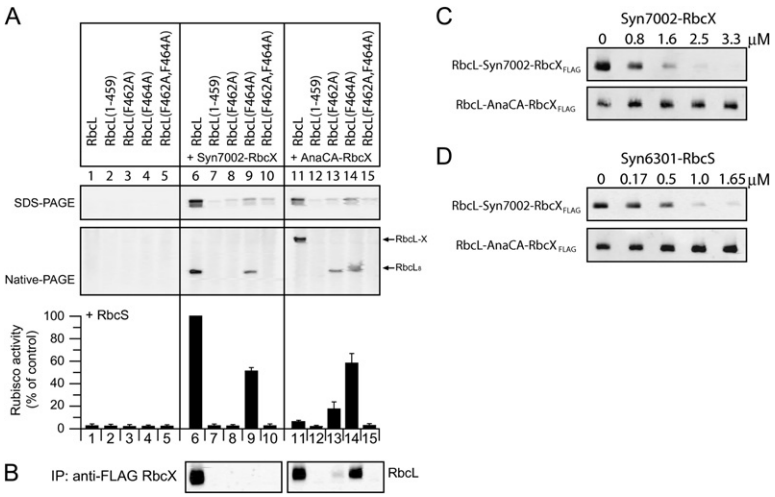

Figure 5. Effects of Modulating RbcX Binding Strength on RbcL Assembly

(A) Syn7002-RbcL or C-terminal mutants indicated were expressed in *E. coli* either alone or with Syn7002-RbcX or AnaCA-RbcX. Soluble fractions of cell lysates were analyzed for RbcL (SDS-PAGE), $RbcL_8$ (Native-PAGE), and carboxylation activity as in Figure 1B. Error bars indicate standard deviation of three independent experiments.

(B) Soluble lysates from coexpression of Syn7002-RbcL wild-type or mutants with Syn7002-$RbcX_{FLAG}$ or AnaCA-$RbcX_{FLAG}$ were subjected to immunoprecipitation with anti-FLAG affinity beads. Coimmunoprecipitated RbcL was detected by immunoblotting with RbcL antibody.

(C and D) Dynamic nature of the $RbcL_8$-RbcX interaction. Complexes of Syn7002-RbcL/Syn7002-$RbcX_{FLAG}$ or Syn7002-RbcL/AnaCA-$RbcX_{FLAG}$ produced by coexpression in *E. coli* were immunoprecipitated from soluble lysate as in (B). The immunobeads were then incubated with the indicated concentrations of purified nontagged Syn7002-RbcX (C) or RbcS (D) for 15 min at room temperature. Bound RbcL was eluted and analyzed by SDS-PAGE and immunoblotting.

axis of the RbcX dimer, indicating that one orientation is markedly preferred in the asymmetric environment of the crystal lattice. In the refined model, the peptide adopts an extended conformation with the side chains F462 and F464 extending into cavities lined by the side chains of T13, Y17, Y20, I50, and Q51 at the center of the RbcX cleft; the polar side chains of the peptide face outwards and are mostly disordered (Figures 4C and 4D). I460 of the peptide appears to contact Y20, R24, and S45 of one RbcX chain. In addition, the observed geometry is compatible with three hydrogen bonds formed between the peptide backbone and the side chains of Y20, R24, and Q51. The conformations of the two Q51 side chains appear to be mainly governed by van der Waals contacts to the phenyl rings of peptide residues F462 and F464 (Figure 4D).

Binding analysis by isothermal titration calorimetry (Figure S9) revealed a relatively low affinity of Syn7002-RbcX for peptide EIKFEFD (K_D ~230 μM), comprising the core binding region. A somewhat higher affinity (K_D ~ 160 μM) was measured with the longer peptide KEIKFEFDTVD, which includes the conserved residues Lys458 and Asp468. These measurements indicate that the interaction of Syn7002-RbcX with the RbcL C terminus is highly dynamic. Interestingly, substantially higher affinities for these peptides were measured with AnaCA-RbcX (K_D ~ 60 μM and 5 μM, respectively). In AnaCA-RbcX, the loop region between helices α2 and α3 is shorter by one residue and contains a lysine at position 49, thus introducing a positive charge in the proximity of the binding groove (Figures S6B and S6C). The positioning of this lysine may result in an increased affinity for the negatively charged C terminus of RbcL.

Next, RbcL C-terminal mutants were analyzed to assess the significance of the RbcL C terminus for assembly. As shown above, wild-type RbcL produced soluble $RbcL_8$ complex competent for association with RbcS in a manner dependent on Syn7002-RbcX (Figure 5A, lanes 1 and 6). Immunoblotting of the $RbcL_8$ complex detected on Native-PAGE did not reveal the presence of RbcX (data not shown), consistent with the labile nature of the $RbcL_8$-RbcX interaction, while immunoprecipitation of $RbcX_{FLAG}$ from cell extracts coimmunoprecipitated a substantial amount of RbcL (Figure 5B). In contrast, expression of RbcL(1–459), lacking the C-terminal recognition sequence for RbcX, did not result in soluble protein despite the presence of RbcX (Figure 5A, lane 7). Individual or combined mutation of F462 and F464 confirmed the critical nature of these residues. Whereas RbcL(F462A) and RbcL(F462A,F464A) prevented the formation of $RbcL_8$ (Figure 5A, lane 8 and 10), RbcL(F464A) still allowed the production of a reduced amount of soluble and assembled protein (Figure 5A, lane 9). Thus, F462 appears to be more important in anchoring the RbcL C terminus to RbcX. Notably, deletion of the C-terminal peptide from Syn6301-RbcL abolished the RbcX-independent assembly of this protein, suggesting a direct role of the C terminus in $RbcL_8$ assembly or stability beyond serving as a RbcX docking site (Figure S1B).

Dynamic Nature of RbcX-RbcL Interaction Is Critical for Holoenzyme Assembly

The difference in affinities for the RbcL C terminus observed with Syn7002-RbcX and AnaCA-RbcX (Figure S9) allowed us to determine the functional relevance of the

dynamic nature of this interaction. Surprisingly, AnaCA-RbcX, while supporting the expression of soluble Syn7002-RbcL, failed to promote the formation of $RbcL_8$ complexes competent for assembly with RbcS (Figure 5A, lane 11). Instead, a high-molecular-weight form of RbcL (RbcL-X) was detected which was tightly associated with AnaCA-RbcX by coimmunoprecipitation (Figure 5B and data not shown). A similar high-molecular-weight complex was observed upon binding of AnaCA-RbcX to preformed Syn6301 $RbcL_8$ (Figure S10). Based on static light scattering, the mass of this complex was ~730 kDa, consistent with eight to nine RbcX dimers bound per $RbcL_8$ (Figure S2B). Formation of this nonproductive complex was not observed with RbcL(1–459) or the RbcL(F462A,F464A) double mutant (Figure 5A, lanes 12 and 15). Interestingly, a substantial amount of assembly-competent $RbcL_8$ core complex formed upon coexpression of AnaCA-RbcX with the single phenylalanine mutations RbcL(F464A) and RbcL(F462A) (Figure 5A, lanes 13 and 14). Thus, attenuating the affinity of the heterologous AnaCA-RbcX for the RbcL C terminus restored productive assembly. As revealed by coimmunoprecipitation, RbcL(F464A) interacted more strongly with AnaCA-RbcX than with RbcL(F462A), confirming the dominant role of F462 (Figure 5B).

Next, we analyzed the exchangeability of RbcX-bound $RbcL_8$. To this end, RbcL was coexpressed with either FLAG-tagged Syn7002-RbcX or AnaCA-RbcX, and the respective complexes were immunoprecipitated as in Figure 3C. Bound $RbcL_8$ was detected by immunoblotting after incubation with increasing concentrations of nontagged Syn7002-RbcX. Half-maximal displacement of RbcL was observed with ~1 μM RbcX, providing an estimate for the apparent affinity of Syn7002-RbcX for $RbcL_8$. Complete displacement of $RbcL_8$ by higher RbcX concentrations occurred within the 15 min incubation time. Thus, the peripheral surface of RbcX contributes to $RbcL_8$ binding over the lower affinity of the central peptide cleft alone (K_D ~ 150 μM). Nevertheless, the $RbcL_8$-RbcX interaction appears to retain a substantial off rate, consistent with the dissociation of the complex upon gel filtration (Figure 3C). In contrast, Syn7002-RbcX failed to displace $RbcL_8$ from the complex with AnaCA-$RbcX_{FLAG}$ (Figure 5C), presumably due to the 30-fold higher affinity of AnaCA-RbcX for the RbcL C terminus. In an analogous experiment, the displacement reaction was performed with RbcS, which binds to free $RbcL_8$ with an affinity of ~10 nM (Andrews, 1988). $RbcL_8$ was readily displaced from Syn7002-RbcX by submicromolar RbcS concentrations (Figure 5D). In contrast, RbcS failed to displace $RbcL_8$ from the complex with AnaCA-RbcX (Figure 5D), explaining the nonproductive nature of the latter. Importantly, bound RbcS was not displaced from $RbcL_8$ even by a 20-fold excess of RbcX, as detected by gel filtration analysis (data not shown). These results support the conclusion that complex formation between RbcL and RbcX must be dynamic in order to support Rubisco holoenzyme formation.

RbcX Action Begins Early in RbcL Assembly

$RbcL_8$ assembly is thought to involve the formation of dimers which then associate to tetramers (Hubbs and Roy, 1993). At which stage does RbcX begin to interact in this reaction? To address this question, RbcL was translated in vitro in *E. coli* lysate supplemented with GroEL/GroES and $RbcX_{FLAG}$. Translation was first performed for 6 min in the absence of labeled amino acid to ensure linear RbcL production, followed by a 6 min pulse with ^{35}S-methionine and a chase with excess unlabeled methionine for up to 160 min. Aliquots of the reaction were withdrawn at different times, stopped on ice, and then analyzed by a discontinuous Bis-Tris Native-PAGE system in which protein migration correlates well with molecular mass. In the absence of RbcX, GroEL-bound RbcL (~800 kDa) was visible at the beginning of the chase, followed by the appearance of a fuzzy low-molecular-weight band that migrated similarly to a monomeric mutant form of bacterial Rubisco from *R. rubrum* (50 kDa; Figure 6A). This band contained full-length RbcL, as demonstrated by excision and reanalysis by SDS-PAGE (data not shown) and thus represented RbcL monomers. In addition, a sharp RbcL band migrating similarly to dimeric Rubisco from *R. rubrum* was observed. In the presence of excess Syn7002-RbcX, these forms of RbcL decreased over time, and formation of $RbcL_8$ occurred (Figure 6B). However, no RbcX-bound assembly intermediates were detected, perhaps due to the dynamic nature of the RbcL-RbcX interaction.

Indeed, when the same experiment was performed with AnaCA-RbcX, two slower-migrating forms of RbcL ($RbcL\text{-}I_1$ and $RbcL\text{-}I_2$) in the range of 200–350 kDa were detected in equilibrium with RbcL monomer and dimer. RbcL monomer was more efficiently cleared from GroEL and more quantitatively consumed than in the assembly reaction with Syn7002-RbcX. Immunoprecipitation with anti-FLAG antibody confirmed that AnaCA-RbcX interacted with RbcL early during assembly (data not shown). The appearance of $RbcL\text{-}I_1$ and $RbcL\text{-}I_2$ was followed by the formation of high-molecular-weight $RbcL_8$-RbcX complex (~730 kDa) that migrated close to GroEL (Figure 6C). Notably, formation of $RbcL\text{-}I_1$ and $RbcL\text{-}I_2$ was not observed upon translation of RbcL(F462A,F464A) mutant protein (Figure 6D), indicating that recognition of the C-terminal motif initiates the interaction of RbcX with RbcL. Based on these findings, RbcX appears to engage newly-synthesized RbcL subunits immediately after their chaperonin-assisted folding at the level of monomers or dimers, shifting the equilibrium toward RbcX-bound intermediates and promoting the formation of $RbcL_8$ core complexes.

DISCUSSION

In this study we have defined RbcX as an assembly chaperone of cyanobacterial form I Rubisco, an abundant hexadecameric enzyme very similar to Rubisco of higher plants. RbcX interacts with RbcL subunits subsequent to their GroEL/GroES-mediated folding (Figure 7, step 1).

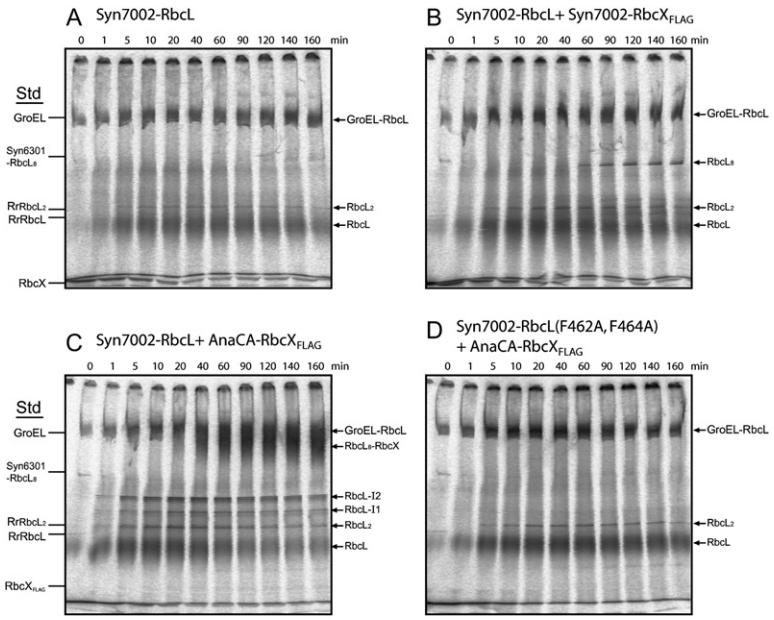

Figure 6. Pulse-Chase Analysis of RbcL Assembly upon In Vitro Translation

Pulse-chase translation of Syn7002-RbcL was performed as described in Experimental Procedures in the absence of RbcX (A), presence of Syn7002-$RbcX_{FLAG}$ (B), or AnaCA-$RbcX_{FLAG}$ (C). Syn7002-RbcL(F462A,F464A) was translated in the presence of AnaCA-$RbcX_{FLAG}$ (D). Reactions were stopped at the chase times indicated, then analyzed by discontinuous Bis-Tris Native-PAGE and autoradiography. Positions of protein standards are indicated.

Folded RbcL monomers may spontaneously form dimers or interact with RbcX immediately upon release from GroEL, resulting in stabilization of assembly intermediates competent for efficient progression to $RbcL_8$ core particles (Figure 7, steps 2 and 3). Specific recognition of the C-terminal RbcL peptide by a central RbcX-binding cleft is critical in this process; it results in shielding of the hydrophobic side chains of this sequence and serves to position peripheral binding surfaces of RbcX in proximity to RbcL. The complex between RbcL and RbcX is dynamic, facilitating the eventual displacement of RbcX by RbcS subunits to form the functional holoenzyme (Figure 7, step 4). RbcX is distinct from promiscuous folding chaperones such as Hsp70 or GroEL in that it recognizes structural features specific to RbcL. While the dependence on RbcX may vary among Rubisco homologs, the conservation of the C-terminal RbcX recognition motif in RbcL sequences suggests a general role of RbcX in ensuring efficient form I Rubisco assembly. The RbcX mechanism may serve as a paradigm in understanding how cellular machinery can promote the efficient formation of complex oligomeric structures.

RbcX Structure and Mechanism

A key feature of the arc-shaped RbcX dimer is a central binding cleft for the C-terminal peptide of RbcL, encompassing the sequence EIKFEFD (residues 459 to 465 in Syn7002-RbcL). The peptide is bound in an extended conformation with the side chains F462 and F464 occupying hydrophobic pockets of the RbcX cleft. In addition, hydrogen bonds between the peptide backbone and RbcX residues lining the groove contribute to specific binding. Although RbcX is all α helical, this binding mode is generally reminiscent of the interaction of extended hydrophobic peptides with the β sandwich-binding cleft of the general chaperone Hsp70 (Zhu et al., 1996). However, bacterial Hsp70, DnaK, failed to bind the C-terminal RbcL peptide (data not shown), consistent with the exclusion of negatively charged amino acid residues by DnaK (Rüdiger et al., 1997). As the ends of polypeptide chains are often surface exposed, specific recognition of N- or C-terminal segments may be employed more generally by assembly chaperones.

How does binding of the C-terminal RbcL peptide by RbcX promote Rubisco assembly? Given its high degree

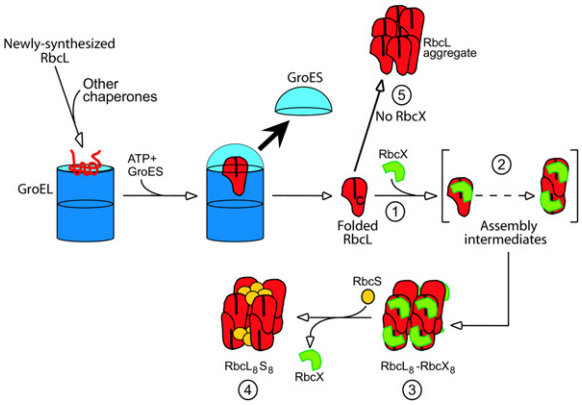

Figure 7. Working Model of RbcX Function in Cyanobacterial Rubisco Assembly

RbcX functions to increase the efficiency of Rubisco assembly by acting on folded RbcL subunits subsequent to their GroEL/GroES-mediated folding. Recognition of RbcX requires the exposed C-terminal RbcL peptide (see Discussion for details and Figure S11). Note that assembly of $RbcL_8S_8$ may also occur independently of RbcX for some Rubisco homologs, presumably involving similar assembly intermediates.

of conservation among hexadecameric Rubisco large subunits, this segment is likely to have an important structural and/or functional role. Because disruption of peptide binding abolished the formation of soluble, assembly-competent RbcL protein, RbcX appears to protect this sequence from undergoing aberrant interactions. Interestingly, C-terminal truncation or mutation of RbcL also disrupted the RbcX-independent, but inefficient, assembly of Syn6301-RbcL (Figure S1B and data not shown), indicating a direct role of the C-terminal element in forming or stabilizing the $RbcL_8$ core complex. Being located on the outer surface of assembled Rubisco, the C-terminal peptide is assumed to have a regulatory function in catalysis. It is thought to cycle during the enzymatic reaction between a more open conformation and a tightly bound state, stabilizing the lid segment of the active site to enclose the substrate ribulose-bisphosphate (or the transition state analog, carboxyarabinitol bisphosphate [CABP]; Duff et al., 2000; Zhu et al., 1998). Formation of the closed state involves Asp468, immediately adjacent to the RbcX-recognition motif. In the crystal structure of Rubisco from Syn6301 (in complex with CABP; Figure S11A), the C-terminal RbcL peptide is not covered by RbcS but would nevertheless be inaccessible to RbcX as it is not sufficiently detached from the complex, and its hydrophobic side chains are only partially solvent exposed. Thus, RbcX may interact with the C-terminal sequence until its attachment to the main body of Rubisco occurs.

The central RbcX-binding cleft functions in cooperation with polar binding surfaces around the corners of the RbcX dimer. Mutation of the peripheral region in RbcX mutant Q29A impaired RbcL assembly in a manner distinct from that observed upon disabling the central peptide cleft. Soluble but misassembled RbcL of >800 kDa formed under these conditions (Figure 3B), suggesting that the peripheral RbcX surface promotes the proper alignment of RbcL dimers for efficient construction of $RbcL_8$ complexes, ultimately to be stabilized by RbcS (Curmi et al., 1992). Binding to the RbcL C terminus would serve as an anchor to position the peripheral binding surfaces, perhaps allowing RbcX to bridge adjacent RbcL subunits. Assuming the α helix preceding the C-terminal binding motif in RbcL remains in place, one edge of RbcX would be able to contact the gap between adjacent RbcL dimers, which is occupied by RbcS in the holoenzyme structure (Figure S11). How exactly RbcL interacts with the corner regions of RbcX remains to be defined, but an overlap of RbcX- and RbcS-binding regions could contribute to efficient RbcX displacement.

Dynamic Nature of RbcX Function

Binding and release of RbcX from its substrate is independent of ATP-regulated conformational changes. Our data suggest that the interaction between cognate RbcX and $RbcL_8$ has a sufficiently fast off rate to allow for efficient displacement of RbcX by RbcS, which binds stably to $RbcL_8$ (Andrews, 1988). While the binding constants of RbcX for the C-terminal RbcL peptide alone are in the 100 μM range, the overall affinity of RbcX for the $RbcL_8$ core complex appears to be close to 1 μM (Figure 5C). Thus, the polar corner surface of RbcX contributes substantially to overall binding, presumably facilitated by the occurrence of this region on both ends of the symmetrical RbcX dimer. However, the peripheral sites alone fail to maintain a stable interaction with RbcL. Thus, combining two structurally independent, relatively weak interaction sites would provide biologically relevant binding strength coupled with high dynamics, a strategy that may be followed more generally by assembly chaperones to achieve efficient product release.

Importantly, the binding parameters of the RbcX-$RbcL_8$ interaction (and similarly the RbcS-$RbcL_8$ interaction) appear to have been optimized for the proteins from the same organism in order to facilitate RbcX recycling. As a consequence, exchangeability of the proteins between organisms is limited despite their close evolutionary relationship. Combining Syn7002-RbcL with the RbcX from *Anabaena* sp. CA, which binds the C-terminal RbcL-peptide with ~30-fold higher affinity, demonstrated the significance of this adaptation. Formation of a stable complex, most likely $RbcL_8$-$RbcX_8$, was observed with AnaCA-RbcX, from which RbcX could not be displaced by RbcS. This dead-end complex presumably defines the otherwise transitory end-state of RbcX activity in the assembly pathway prior to entry of RbcS (Figure 7).

Implications for Rubisco Assembly in Higher Plants

Hexadecameric form I Rubisco is thought to have evolved from the simpler dimeric form II as an adaptation to the increased oxygen and lowered carbon dioxide atmosphere. The resulting increase in structural complexity may explain the need for a specific assembly chaperone, particularly when considering the complex role of the C-terminal RbcL segment in assembly and catalysis of form I Rubisco (Zhu et al., 1998). Indeed, the C-terminal RbcX recognition sequence is conserved in higher plant RbcL, and homologs to RbcX genes are present in plant genomes exhibiting 29% similarity to the cyanobacterial RbcX sequences (Figure S3). It is thus likely that RbcX has an important role in the assembly process of plant Rubisco, which is faced with the additional difficulty that RbcS subunits must be imported into chloroplasts to assemble with RbcL synthesized within the organelle (Roy, 1989). The failure of heterologous form I Rubiscos to assemble upon transgenic expression in plants (Andrews and Whitney, 2003) may suggest an incompatibility of these enzymes with plant RbcX. Future attempts to improve the catalytic properties of crop plant Rubisco through protein engineering may have to take the function of RbcX into consideration.

EXPERIMENTAL PROCEDURES

Plasmids and Proteins

Plasmid constructs for expression of Rubisco and RbcX wild-type and mutant proteins from cyanobacterial species *Synechococcus* sp. PCC7002, *Synechococcus* sp. PCC6301, and *Anabaena* sp. CA, as

well as the expression and purification of chaperone and Rubisco proteins, are described in Supplemental Experimental Procedures.

In Vivo Assembly of Syn7002-RbcL or Syn7002-RbcLS in *E. coli*

Expression of RbcL, RbcL/X, RbcL/S, or RbcL/X/S from the respective pET-vectors was induced by IPTG in *E. coli* BL21(DE3) cells grown to mid-log phase (1 mM IPTG, ~3.5 hr at 30°C) with or without prior transient overexpression of GroEL and GroES from a tetracycline-inducible promoter of the plasmid pG-*KJE8* (20 ng/ml tetracycline, 2 hr at 30°C). Equivalent amounts of cells were lysed by ultrasonication and fractioned into soluble and insoluble fractions by centrifugation (20,800 × g, 30 min at 4°C). Soluble lysate fractions were analyzed for assembled RbcL by 6% Native-PAGE, followed by immunoblotting with RbcL-specific antibody (AgriSera). Rubisco carboxylation activity in the soluble lysate fractions was measured essentially as described (Goloubinoff et al., 1989b; see Supplemental Experimental Procedures).

In Vitro Translation of Rubisco

Translations were carried out in the coupled RTS100 HY *E. coli* transcription/translation system (Roche) from T7-promoter-driven plasmids in the presence of ^{35}S-Met or unlabeled methionine (Agashe et al., 2004). Translation reactions were run for 1.5 hr at 30°C unless stated otherwise and were stopped with chloramphenicol (CAM; 200 μg/ml, 2 min on ice). Purified proteins were added to the translation lysate at the concentrations indicated in figure legends. Posttranslational addition of proteins was performed after CAM addition, followed by transfer of reactions to 30°C for further incubation as indicated. Reactions were separated into soluble and insoluble fractions by centrifugation and analyzed on 12.5% SDS-PAGE or 6% Native-PAGE, followed by autoradiography.

When indicated, GroEL was immunodepleted from the translation mix by incubation with polyclonal GroEL antibody bound to Protein A Sepharose beads (Amersham) by gentle shaking for 45 min at 4°C and removal of beads by centrifugation. Efficient depletion of GroEL was confirmed by immunoblotting with GroEL antibody.

In pulse-chase experiments translation of Syn7002-RbcL was carried out in the presence of GroEL/GroES (0.5/1.0 μM) and purified RbcX (40 μM) for 6 min at 30°C before addition of ^{35}S-Met for 6 min. The chase was started by addition of 3 mM unlabeled methionine. Aliquots were collected at the time points indicated in the figure legend. Soluble protein was analyzed by discontinuous Bis-Tris Native-PAGE (Hansen et al., 1999), followed by autoradiography.

Immunoprecipitation and Gel Filtration

$RbcX_{FLAG}$ was immunoprecipitated from soluble cell lysates containing coexpressed RbcL and RbcX with anti-FLAG M2 Affinity Gel Beads (Sigma) by overnight incubation at 4°C. When indicated, bound protein was eluted under native conditions by incubating the beads for 30 min on ice with 100 μl of 3× FLAG peptide solution (Sigma; 300 μg/ml). Cell lysates or FLAG-eluted immunoprecipitates were analyzed on a Superdex 200 column in 50 mM Tris-HCl pH 8.0, 50 mM NaCl, and 5 mM $MgCl_2$. Fractions of 250 μl were TCA precipitated and analyzed by immunoblotting.

Crystallography and Structure Analysis

Production of SeMet labeled RbcX protein, crystallization, and structure determination are described in Supplemental Experimental Procedures. Coordinates and structure factor amplitudes were deposited to Protein Data Bank under accession codes 2PEI, 2PEJ, 2PEK, 2PEM, 2PEN, 2PEQ, and 2PEO.

Peptide-Binding Assay

Binding of $RbcX_{FLAG}$ to an array of dodecapeptides covering the sequence of Syn7002-RbcL and isothermal calorimetry were performed essentially as described (Rüdiger et al., 1997; Wiseman et al., 1989; see Supplemental Experimental Procedures for details).

Supplemental Data

Supplemental Data include Experimental Procedures, References, one table, and 11 figures and can be found with this article online at http://www.cell.com/cgi/content/full/129/6/1189/DC1/.

ACKNOWLEDGMENTS

We thank the JSBG staff at ESRF and E. Pohl at SLS-beamline X10SA-PX-II for their generous help during data collection, M. Stemp for help with the in vitro translation experiments, and F. R. Tabita for Rubisco plasmids. This work was supported by the Deutsche Forschungsgemeinschaft, the Ernst-Jung Foundation, and the Körber Foundation.

Received: February 5, 2007
Revised: March 25, 2007
Accepted: April 10, 2007
Published: June 14, 2007

REFERENCES

Agashe, V.R., Guha, S., Chang, H.C., Genevaux, P., Hayer-Hartl, M., Stemp, M., Georgopoulos, C., Hartl, F.U., and Barral, J.M. (2004). Function of trigger factor and DnaK in multidomain protein folding: Increase in yield at the expense of folding speed. Cell *117*, 199–209.

Andersson, I., and Taylor, T.C. (2003). Structural framework for catalysis and regulation in ribulose-1,5-bisphosphate carboxylase/oxygenase. Arch. Biochem. Biophys. *414*, 130–140.

Andrews, T.J. (1988). Catalysis by cyanobacterial ribulose-bisphosphate carboxylase large subunits in the complete absence of small subunits. J. Biol. Chem. *263*, 12213–12219.

Andrews, T.J., and Lorimer, G.H. (1985). Catalytic properties of a hybrid between cyanobacterial large subunits and higher plant small subunits of ribulose bisphosphate carboxylase-oxygenase. J. Biol. Chem. *260*, 4632–4636.

Andrews, T.J., and Lorimer, G.H. (1987). Rubisco: structure, mechanisms, and prospects for improvement. In In The Biochemistry of Plants: A Comprehensive Treatise, *Volume 10*, M.D. Hatch and N.K. Boardman, eds. (New York: Academic Press), pp. 131–218.

Andrews, T.J., and Whitney, S.M. (2003). Manipulating ribulose bisphosphate carboxylase/oxygenase in the chloroplasts of higher plants. Arch. Biochem. Biophys. *414*, 159–169.

Barraclough, R., and Ellis, R.J. (1980). Protein synthesis in chloroplasts. IX. Assembly of newly-synthesized large subunits into ribulose bisphosphate carboxylase in isolated intact pea chloroplasts. Biochim. Biophys. Acta *608*, 18–31.

Brinker, A., Pfeifer, G., Kerner, M.J., Naylor, D.J., Hartl, F.U., and Hayer-Hartl, M. (2001). Dual function of protein confinement in chaperonin-assisted protein folding. Cell *107*, 223–233.

Corpet, F. (1988). Multiple sequence alignment with hierarchical clustering. Nucleic Acids Res. *16*, 10881–10890.

Curmi, P.M., Cascio, D., Sweet, R.M., Eisenberg, D., and Schreuder, H. (1992). Crystal structure of the unactivated form of ribulose-1,5-bisphosphate carboxylase/oxygenase from tobacco refined at 2.0 Å resolution. J. Biol. Chem. *267*, 16980–16989.

Duff, A.P., Andrews, T.J., and Curmi, P.M. (2000). The transition between the open and closed states of Rubisco is triggered by the inter-phosphate distance of the bound bisphosphate. J. Mol. Biol. *298*, 903–916.

Ellis, R.J. (2006). Molecular chaperones: assisting assembly in addition to folding. Trends Biochem. Sci. *31*, 395–401.

Emlyn-Jones, D., Woodger, F.J., Price, G.D., and Whitney, S.M. (2006). RbcX can function as a Rubisco chaperonin, but is non-essential in Synechococcus PCC7942. Plant Cell Physiol. *47*, 1630–1640.

Frydman, J. (2001). Folding of newly translated proteins in vivo: The role of molecular chaperones. Annu. Rev. Biochem. *70*, 603–647.

Goloubinoff, P., Christeller, J.T., Gatenby, A.A., and Lorimer, G.H. (1989a). Reconstitution of active dimeric ribulose bisphosphate carboxylase from an unfolded state depends on two chaperonin proteins and MgATP. Nature *342*, 884–889.

Goloubinoff, P., Gatenby, A.A., and Lorimer, G.H. (1989b). GroE heat-shock proteins promote assembly of foreign prokaryotic ribulose bisphosphate carboxylase oligomers in Escherichia coli. Nature *337*, 44–47.

Gutteridge, S., and Gatenby, A.A. (1995). Rubisco synthesis, assembly, mechanism, and regulation. Plant Cell *7*, 809–819.

Hansen, W.J., Cowan, N.J., and Welch, W.J. (1999). Prefoldin-nascent chain complexes in the folding of cytoskeletal proteins. J. Cell Biol. *145*, 265–277.

Hartl, F.U., and Hayer-Hartl, M. (2002). Molecular chaperones in the cytosol: from nascent chain to folded protein. Science *295*, 1852–1858.

Hill, J.E., and Hemmingsen, S.M. (2001). Arabidopsis thaliana type I and II chaperonins. Cell Stress Chaperones *6*, 190–200.

Hubbs, A.E., and Roy, H. (1993). Assembly of in vitro synthesized large subunits into ribulose-bisphosphate carboxylase/oxygenase. Formation and discharge of an L8-like species. J. Biol. Chem. *268*, 13519–13525.

Larimer, F.W., and Soper, T.S. (1993). Overproduction of Anabaena 7120 ribulose-bisphosphate carboxylase/oxygenase in Escherichia coli. Gene *126*, 85–92.

Li, L.-A., and Tabita, F.R. (1997). Maximum activity of recombinant ribulose 1,5-bisphosphate carboxylase/oxygenase of anabaena sp. strain ca requires the product of the rbcX gene. J. Bacteriol. *179*, 3793–3796.

Onizuka, T., Endo, S., Akiyama, H., Kanai, S., Hirano, M., Yokota, A., Tanaka, S., and Miyasaka, H. (2004). The rbcX gene product promotes the production and assembly of ribulose-1,5-bisphosphate carboxylase/oxygenase of Synechococcus sp. PCC7002 in Escherichia coli. Plant Cell Physiol. *45*, 1390–1395.

Roy, H. (1989). Rubisco assembly: a model system for studying the mechanism of chaperonin action. Plant Cell *1*, 1035–1042.

Rüdiger, S., Germeroth, L., Schneider-Mergener, J., and Bukau, B. (1997). Substrate specificity of the DnaK chaperone determined by screening cellulose-bound peptide. EMBO J. *16*, 1501–1507.

Tabita, F.R. (1999). Microbial ribulose 1,5-bisphosphate carboxylase/oxygenase: a different perspective. Photosynth. Res. *60*, 1–28.

Wiseman, T., Williston, S., Brandts, J.F., and Lin, L.N. (1989). Rapid measurement of binding constants and heats of binding using a new titration calorimeter. Anal. Biochem. *179*, 131–137.

Zhu, G.H., Jensen, R.G., Bohnert, H.J., Wildner, G.F., and Schlitter, J. (1998). Dependence of catalysis and CO_2/O_2 specificity of Rubisco on the carboxy-terminus of the large subunit at different temperatures. Photosynth. Res. *57*, 71–79.

Zhu, X.T., Zhao, X., Burkholder, W.F., Gragerov, A., Ogata, C.M., Gottesman, M.E., and Hendrickson, W.A. (1996). Structural analysis of substrate binding by the molecular chaperone DnaK. Science *272*, 1606–1614.

Accession Numbers

Coordinates and structure factor amplitudes were deposited to Protein Data Bank under accession codes 2PEI, 2PEJ, 2PEK, 2PEM, 2PEN, 2PEQ, and 2PEO.